

Episodic accretion around the Herbig Ae star BF Orionis^{*}

Evidence for the presence of extra-solar comets

D. de Winter^{1,2,**}, C.A. Grady³, M.E. van den Ancker⁴, M.R. Pérez⁵, and C. Eiroa¹

¹ Departamento Física Teórica, C-XI, Facultad de Ciencias, Universidad Autónoma de Madrid, Cantoblanco, E-28049 Madrid, Spain

² Centro de Astrofísica de Universidade do Porto, Rua Campo Alegre 823, 4150 Porto, Portugal

³ Eureka Scientific, 2452 Delmar St., Suite 100, Oakland, CA 94602, USA

⁴ Astronomical Institute “Anton Pannekoek”, University of Amsterdam, Kruislaan 403, 1098 SJ Amsterdam, The Netherlands

⁵ Space Applications Corp., 9315 Largo Drive West, Suite 250, Largo MD 20774, USA

Received 5 June 1998 / Accepted 2 December 1998

Abstract. The results of a monitoring programme of high and intermediate resolution spectra covering He I 5876 Å, Na I $D_{2,1}$ and H α of the isolated Herbig Ae star BF Ori are presented. We detect the presence of blue and redshifted emission and absorption components of these lines which vary from day-to-day with correlated changes suggesting a similar origin.

The appearance, strength and variations of the redshifted Na I D absorption component on a time scale of days show variable accretion activity similar to that seen toward the Herbig Ae star UX Ori and β Pic, suggesting evaporation of star-grazing bodies. We estimate for one event that such a body is kilometer sized, evaporates at a distance of about 0.4 AU from the central star and has a mass comparable to comets in the solar system.

A dependence was found of the H α line profile on the photometric brightness of BF Ori similar to that observed for UX Ori. It is evidence for obscuration of a dense dusty body located in the outer disk regions as no extra absorption components from a gaseous content and no direct influences on the cometary activity were observed. More complex variations of the H α profile could be explained in part by absorption of star-grazer material, equal to the absorption at the sodium lines, and in part by obscuration of its line forming region by the cometesimal. More evidences for detections of revolving clumpy material are: observed changes in the velocity direction of the very strong Na I $D_{2,1}$ low velocity absorption components and the observed flip over of the relative strength of the blue and red peak of H α simultaneous with the change of blue to redshifted absorption components in both the Na I $D_{2,1}$ and He I lines. In case of orbiting bodies, the estimated period lies between 60 and 100 days with a distance from 0.35 to 0.57 AU, respectively.

The detection of possible orbiting and comet-like objects in the disk of BF Ori, a 3^{+2}_{-1} Myr old pre-main sequence A5–6 IIIe

star, making it a possible progenitor of the HR 4796 (protoplanetary) disk system, suggests the existence of structures similar to those probably present in the solar system at a time of formation of planetesimals. The estimated much higher than cosmic abundances of refractory (Na) over volatile (H, He) gases for the detected bodies supports this suggestion.

Key words: comets: general – stars: emission-line – stars: individual: Beta Pic – stars: individual: BF Ori – stars: individual: UX Ori – stars: pre-main sequence

1. Introduction

In the past few years the formation and evolution of planetary systems has moved from theoretical studies to the forefront of observational research with detection, via reflex motion effects, of Jupiter-mass objects in close proximity to nearby Solar-type stars (Mayor & Queloz 1995; Marcy & Butler 1996), and high resolution imaging of dust disks with cleared central cavities around 10–350 Myr old A stars (Holland et al. 1998; Koerner et al. 1998; Jayawardhana et al. 1998). More recently, infrared imaging of the binary system HR 4796 has provided another clear example of a possible protoplanetary disk system around a nearby 8 ± 3 Myr old A-type star (Jura et al. 1993; Stauffer et al. 1995).

Models for planetary system formation predict that such objects should be the end-products of the evolution of gas and dust disks. Promising support for these models is provided by the detection of circumstellar gas and dust disks around young stars (Beckwith & Sargent 1996; Mannings et al. 1997). However, linking the protoplanetary and debris disks to mature planetary systems requires a demonstration that collisionally-grown bodies are routinely produced and resemble our expectations for planetesimals, as noted by Beckwith & Sargent (1996).

Such bodies are exceedingly difficult to detect directly, compared to dust disks, since they lack the large surface area of comparable amounts of micron-sized dust grains. However, they can be indirectly sensed if they approach the star sufficiently close,

Send offprint requests to: D. de Winter
(dolf@astro1.ft.uam.es; dwinter@iac.es)

* Based on observations made at the European Southern Observatory, La Silla, Chile.

** Current address: Instituto de Astrofísica de Canarias, C/ Via Láctea s/n, E-38200 La Laguna, Tenerife, Spain

and in sufficient numbers that a kind of cometary activity occurs. Redshifted circumstellar gas features have been recognized in the optical and UV spectra of β Pic for the past 13 years (Kondo & Bruhweiler 1985; Lagrange et al. 1988; Boggess et al. 1991; Ferlet et al. 1993), and have been most successfully interpreted as the comae of swarms of star-grazing bodies (Beust et al. 1996). The on-going controversy over the age of β Pic (Jura et al. 1993; Backman & Paresce 1993; Lanz et al. 1995; Crifo et al. 1997) means that it is uncertain whether the infall activity in this system reflect planetary formation processes or the evolution of the debris disk following any epoch of these processes. Detection of similar activity in unambiguously younger stars offers the opportunity of probing planetesimals at the epoch of planet formation.

In this paper, we present the results of four spectroscopic monitoring campaigns of one of such a system, BF Ori. Sect. 2 provides a general background and astrophysical parameters for our target. Sect. 3 summarizes the observations. Sect. 4 contains a discussion of the individual line profiles, which are evaluated in the context of the infalling evaporating bodies model. Individual spectral features are discussed in Sect. 5. In Sect. 6 we estimate the dimensions of a comet-like body for the October 1993 observations. The accretion activity of BF Ori is compared with those of other Herbig Ae/Be (HAeBe) stars in Sect. 7. In Sect. 8 we include a discussion on the two possible CS bodies able to interpret the data. Finally Sect. 9 include some concluding remarks.

2. BF Ori: background and astrophysical parameters

The Herbig Ae star BF Ori has a history of large amplitude, photometric variability over $V = 9^m6 - 12^m6$ (Shevchenko et al. 1993), and blueing of the colours during deep minima (Bibo & Thé 1991), similar to that seen in UX Ori and other Herbig Ae stars with strong photometric variability, which Herbst et al. (1994) have termed UXORs. Anti-correlated linear polarization variability consistent with intermittent occultation of the star has been reported by Grinin et al. (1991), implying that the star is viewed close to edge-on through a circumstellar gas and dust disk (Grinin & Rostopchina 1996).

To derive the astrophysical parameters of BF Ori, the total luminosity of BF Ori was computed by integrating over a Kurucz (1991) model for the stellar photosphere, fitted to its extinction-corrected spectral energy distribution (SED). For the construction of this SED, literature data from the ultraviolet to the infrared were combined with unpublished photometry near maximum system brightness. For BF Ori, a spectral type of A5–6 IIIe (van den Ancker et al. 1998), and a distance of 430 ± 60 pc, assuming a membership of Orion OB1 c (Warren & Hesser 1978), were adopted. We then determine the stellar mass and age by comparing the position of the star in the Hertzsprung-Russell diagram with the PMS evolutionary tracks and isochrones by Palla & Stahler (1993). These tracks were calculated for solar metallicity, but we expect no important changes on these estimates for slightly different Z values. The resulting stellar parameters for BF Ori are $\log L_*/L_\odot = 1.37_{-0.13}^{+0.11}$, $M_* = 2.0 \pm 0.2 M_\odot$ and $\log(\text{Age}/\text{yr}) = 6.5 \pm 0.2$.

For comparison purposes, we followed the same procedure for the UXOR prototype UX Ori, adopting a spectral type of A3 IIIe (Timoshenko 1985) and the Orion OB1 distance of 430 ± 60 pc by Warren & Hesser (1978). The results for UX Ori are $\log L_*/L_\odot = 1.47_{-0.13}^{+0.11}$, $M_* = 2.1 \pm 0.2 M_\odot$ and $\log(\text{Age}/\text{yr}) = 6.5 \pm 0.2$. Both UX and BF Ori are thus not only extremely similar in all their observed properties but also in their PMS phase.

In common with other Herbig Ae stars, probably viewed through their disks (Grady et al. 1996), BF Ori exhibits β Pic-like infalling circumstellar gas, and was one of the first Herbig Ae star for which such activity was detected (Welty et al. 1992; Graham 1992). Subsequently, Grinin et al. (1996a) presented for the UXORs WW Vul, RR Tau and BF Ori series of Na I and He I $\lambda 5876$ profiles showing infalling material and correlated changes in these profiles. Their observations, while suggesting a strong parallel with β Pic, did not have the duration and observation frequency to determine whether the infall episodes they reported had a similar duration to such activity in β Pic.

3. Observations

Our observing program consists of high and intermediate resolution spectroscopy obtained during epochs between October 1993 and January 1995. During these runs intensive monitoring could be carried out covering time scales of days and in one occasion even of hours. A detailed observing log of all the spectroscopic observations is given in Table 1.

The high resolution spectra, with $R \approx 50,000 - 55,000$, were all taken with the ESO CAT/CES combination. The equipment and methods used for both the observations and reduction are already described by Grinin et al. (1994) and de Winter et al. (1994). The December 1994 high resolution spectroscopy around Na I were supplemented by intermediate resolution $H\alpha$ spectra ($R \approx 16,500$) taken simultaneously and therefore, only exposed optimally over the 6260–6860 Å range. These observations were taken with the Boller and Chivens spectrograph mounted on the ESO 1.52 m telescope stationed at La Silla. The detector was a Ford Aerospace 2048 × 2048 pixel CCD, with a $15 \times 15 \mu\text{m}$ pixel size. The spectra were reduced using the MIDAS software running under SUN/OS at the ESO headquarters.

4. Analysis of the spectra

In the first subsection the various monitoring data-sets will be analysed. Because of the special character of the December 1994 spectra, exact simultaneous monitoring of all the line profiles, they will be analysed in a second subsection.

4.1. The Na I D, He I & H α line profiles and variations

Na I: In October 1993, when the star was at intermediate brightness level, the Na I D lines, Fig. 1b, were characterized by prominent, high velocity ($v \geq 100 \text{ km s}^{-1}$) redshifted absorption components (RACs) with absorption extending in the red wings up to 200 km s^{-1} . Complex absorption at lower veloc-

Table 1. Journal of Spectral Observations. The magnitudes given are from A.N. Rostopchina (private communications, Ref. 1), unpublished photometry by the authors (Ref. 2) and from A. Miroshnichenko (private communications, Ref. 3).

Date	J.D. +240000	Spectral region	Resolution	Exp. time	No. of spectra	Figure	V	Ref.
'93 Oct. 7–12	9268–9273	H α	50,000	45min	6	1c	11 ^m 7	1
'93 Oct. 8–14	9269–9275	He I & Na I D	55,000	45min	7	1a,b	11 ^m 7	1
'94 Jan. 11	9364	H α	50,000	60min	1	3	–	
'94 Aug. 17	9582	He I & Na I D	55,000	35min	1	2	10 ^m 1	2
'94 Aug. 18	9583	He I & Na I D	55,000	26min	1	2	10 ^m 1	2
'94 Aug. 20	9585	He I & Na I D	55,000	40min	1	2	10 ^m 1	2
'94 Dec. 13–15	9699–9701	H α	16,500	45min	11	4c,5	–	
'94 Dec. 13–16	9699–9702	He I & Na I D	55,000	45min	12	4a,b	–	
'94 Dec. 16	9702	H α	55,000	45min	2	4c	–	
'95 Jan. 15–20	9733–9738	H α	55,000	45min	6	3	10 ^m 2	3

ity is also seen, with the foreground interstellar (IS) absorption visible at $21 \pm 2 \text{ km s}^{-1}$. The profiles exhibit striking day-to-day changes. While all parts of the profiles are variable, the most prominent changes occur for velocities $\geq 100 \text{ km s}^{-1}$, and shortward of the interstellar absorption component. The observed profiles closely resemble those observed in UX Ori for Na I (Grinin et al. 1994), and those seen in other transitions for several H Ae Bes (e.g. Grady et al. 1996; 1997) and β Pic.

Most of the red absorption wings and RACs have a similar shape and depth in both lines of the Na I doublet, being consistent with the presence of optically thick absorption (Grinin et al. 1996a). The RAC profiles on 9 and 10/10/93 are seen up to a maximum depth of $\approx 40\%$ below the continuum level. Comparison of the 1993 October data with the profiles shown in Grinin et al. (1996a), which were obtained closer to optical maximum, shows similar absorption strengths, which means that these features are independent of optical brightness level.

The October 1993 spectra also contain weak blueshifted emission components, especially in the 9 and 13/10/1993 data, which were not detected for UX Ori. Variations in these components are also seen, such as the relatively strong absorption at 10/10/1993 preceded at the 9th by emission in this velocity range.

The sodium line profiles of 17–20 August 1994, Fig. 2b, taken at optical maximum light do not show any RACs. Only several strong sharp absorption components blended with the IS component at $+13 \pm 2 \text{ km s}^{-1}$ are visible. Such components were also detected for UX Ori, but only redshifted. When the strongest absorption components are compared with the data of Grinin et al. (1996a) and those of October 1993, filling in of the low velocity portion of the profile from about 0.9, October 1993, to about 0.6, August 1994, of the continuum level is apparent. These changes and the different velocities measured suggest that this component is not IS, as proposed for UX Ori, but circumstellar.

The August 1994 monitoring covered only three nights but a dynamical sequence seems to be present though. At 17/08/1994, a strong shortward absorption component centered at $-2 \pm 2 \text{ km s}^{-1}$ of which the blue wing extends up to

-40 km s^{-1} is observed. The following night this component becomes slightly weaker, but the velocity ranges are similar. Additionally a weak red wing is visible, stronger than on the 17th, and extending up to $+143 \text{ km s}^{-1}$, a comparable value to that observed at 11/10/1993. The third night the interstellar absorption line is not only accompanied by a blue but also by a redshifted component at $+28 \pm 2 \text{ km s}^{-1}$ both being of comparable strength. The red absorption wing of the sodium lines got even slightly stronger, 20% of the continuum level, and are almost flat from around 0 up to the maximum of $+153 \text{ km s}^{-1}$. The presence of flat bottomed absorption features suggest that the absorption is saturated and does not fully obscure the star. The maximum absorption depth gives a measure of the projected covering onto the stellar disk. As there is no photospheric component for these lines, influences of the stellar rotation (Beust & Lissauer 1994; Hubeny & Heap 1996) on these values are not to be expected.

He I λ 5876: As noted by Grinin et al. (1994), the presence of He I λ 5876 absorption is unexpected in the spectrum of any H Ae star. However, in common to other UXORs with high resolution optical spectra, BF Ori exhibits prominent, variable He I λ 5876 absorption (Grinin et al. 1994, 1996a), which does not exceed a maximum absorption depth of 20% of the local continuum level. In the 1993 October data, Fig. 1a, the prominence of the He I absorption is correlated with the occurrence and strength of the Na I RACs, with the high velocity He I absorption following the Na I velocity distribution. This is best seen for the spectra taken on the 8th, which contains the highest redshifts for both lines, $+280$ and $+250 \text{ km s}^{-1}$ for the He I line and the RACs respectively; and for the almost not redshifted RACs of the 10th, $v_{\text{max}} = +150 \text{ km s}^{-1}$, for which the He I lines extends up to $+170 \text{ km s}^{-1}$. In cases where we have blueshifted emission at the Na I lines, the He I shows a cut-off at relatively low velocities, suggesting either that the He I line may be partially filled in with emission, or that the He I is preferentially associated with the infalling material.

During August 1994, He I 5876 Å is again present in absorption although the strong RACs are absent, Fig. 2a. There

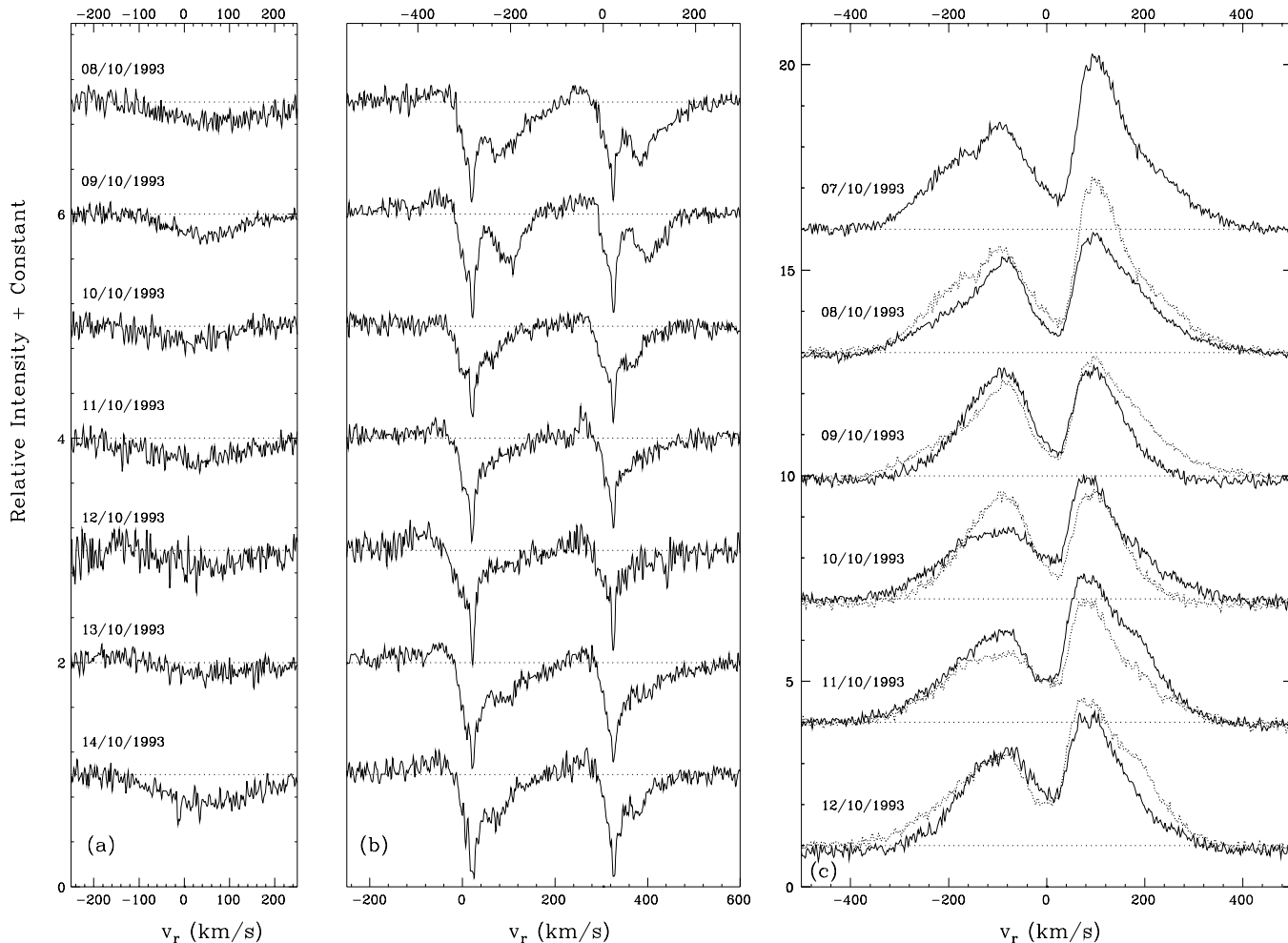


Fig. 1. **a** He I and **b** Na I D line profiles of BF Ori, taken from October 8 to 14, 1993. **c** $H\alpha$ line profiles of BF Ori, taken during October 7–12, 1993. The normalized continuum levels are indicated by thin dotted lines. For the $H\alpha$ spectra the drawn continuum level is influenced by the photospheric absorption line. To visualize the variability the preceding spectrum is plotted by dots.

is a clear co-variation with the development of the red wing of the sodium lines, both in strength and velocity range. The absorption peak is first seen at 0 and in the following two nights at $+18 \text{ km s}^{-1}$, while the extended wings to the red change from $+173$ to $+190$ and finally about $+150 \text{ km s}^{-1}$. Absorption shortwards is seen at remarkable stable velocities of about -180 km s^{-1} . The detections are very similar to that observed for the October 1993 sequence.

H α : Like other UXOR-type HAeBe stars, BF Ori exhibits double-peaked $H\alpha$ emission (Grinin & Rostopchina 1996). Previously published $H\alpha$ data for this star show the red (R) emission component stronger than the violet (V) component in Finkenzeller & Mundt (1984) with the central absorption feature reaching only 1.6 times the local continuum level, and $V > R$ with the central absorption reaching 1.3 times the local continuum in Reipurth et al. (1996). The 1993 October data, Fig. 1c, are similar to the Finkenzeller & Mundt (1984) profile with a weak central absorption, and the red emission component typically stronger than the violet component. The 1995 January data,

Fig. 3, show unusually weak $H\alpha$ emission, with the absorption reversal going below the local continuum level. Such apparent weak emission, relative to the continuum, might be a normalization effect as will be discussed in Sect. 5.1.3.

Night-to-night variations in both the violet and red emission portions of the $H\alpha$ profile are present during the October 1993 and January 1995 series. During both series the largest profile changes are seen on the red emission peak to $+400 \text{ km s}^{-1}$ with $\Delta t \leq 24$ hours. During the October 1993 run, the largest changes at $H\alpha$ coincided with the presence of prominent RAC features in Na I. We notice a diminished red $H\alpha$ component when the RACs are at maximum strength (compare the spectra taken on the 8, 9, 10 and 11/10/1993). On the 8th and 9th the Na I $D_{1,2}$ RACs are strongest and $V/R \approx 1$ for $H\alpha$. The recovery of the red $H\alpha$ component occurs simultaneously with the weakening of the RACs on the 10th and 11th. During the January 1995 series, there are also significant changes in the violet emission out to -200 km s^{-1} with prominent absorption compared to the red peak. Such absorption occurs in the red peak on 19/01/1995 as well, while diminished in the blue peak, causing a slight reversal

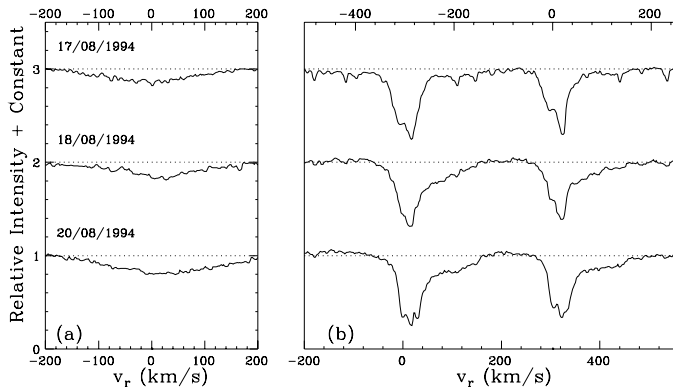


Fig. 2. **a** He I and **b** Na I *D* high resolution line profiles of BF Ori, taken between August 17 and 20, 1994. The continuum levels are again indicated by thin dotted lines.

of the V/R value. A more distinguished reversed H α profile is seen on 11/01/1994, Fig. 3, without any extra absorption components. Despite the variability in other portions of the profile, the depth of the central absorption is not variable during either run for $\Delta t=5-6$ days and even not between the December 1994 and January 1995 run.

4.2. The December, 1994, data

The previous observations confirmed the presence of significant day-to-day variability in all of the observed line profiles of BF Ori, but did not resolve the variability time scale. The 1994 December high and intermediate-resolution run has a monitoring coverage of 3–4 observations per night with regular intervals of about 1 hour (Figs. 4 and 5), being enough to resolve much shorter time scales.

We have no information on the light level, but the S/N in the Na I spectra compared to previous data taken with the same equipment and exposure time, and the strength of the H α self-absorption suggest that these observations were made closer to optical maximum light than the October 1993 data.

4.2.1. The Na I *D*, He I & H α line profiles and variations

The three spectra obtained on 13 December 1994 (JD 9699, top of Fig. 4), are remarkably different from the line profiles discussed before. The Na I *D* lines show blue absorption profiles with wings up to -140 km s $^{-1}$. A similar feature is observed in the He I absorption line. The H α profile during this night is comparable to the one detected on 8/10/1993, with the R \geq V but the R emission peak distributed to lower velocities than in the V peak. The observations clearly indicate a strong correlation between the blue components of these lines. No significant changes between the three different observations, separated by about 2 hours, were detected.

Apart from weak changes, the stability of the line profiles during a night is also seen in the two following ones. However, in comparison with the first night dramatic variations are detected. The central Na I *D* absorption lines are now accompanied by ex-

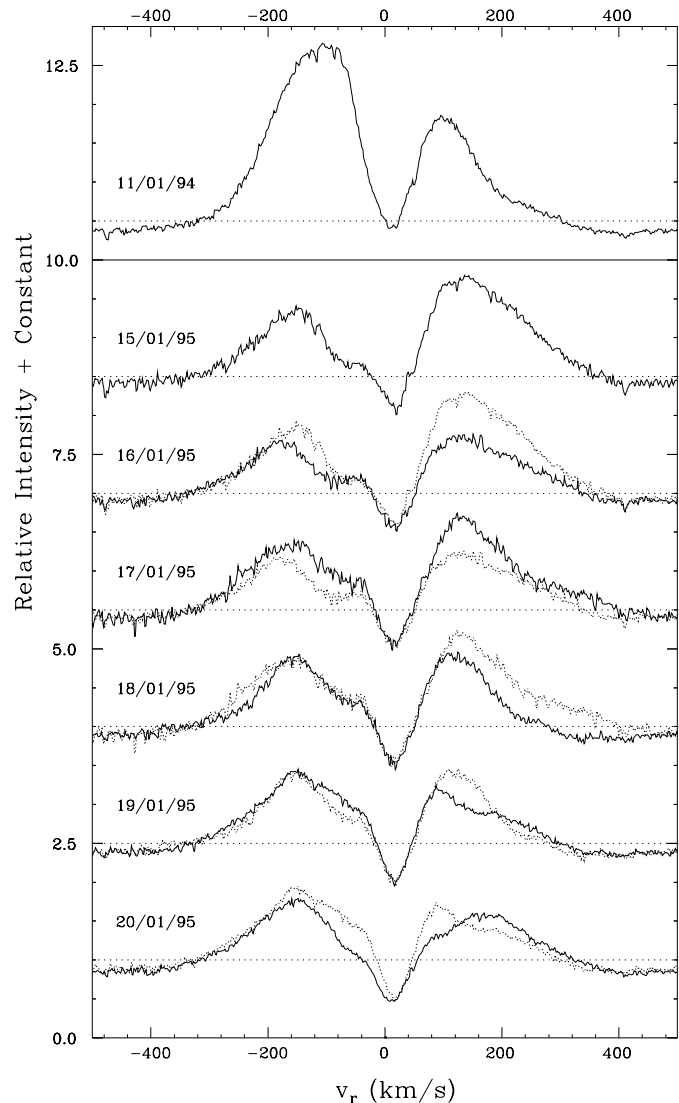


Fig. 3. H α high resolution line profiles of BF Ori, taken on 11 January 1994 (top) and a time series taken between January 15 and 20, 1995. The continuum levels of the surrounding wavelength region are indicated by thin dotted lines; levels which are influenced by the photospheric component. To visualize the variability, the preceding spectrum is plotted by dots.

tended red absorption wings up to $+140$ km s $^{-1}$ (14/12/1994), followed by more developed strong absorption components (15/12/1994) comparable to the October 1993 RACs, which also remain during 16/12/1994. In this last night the redshifted absorption is accompanied by a somewhat stronger absorption in the blue, at low velocities, than at 15/12/1994. Also blueshifted emission is seen during 14 and 15/12/1994, extending up to $+150$ km s $^{-1}$, with small variations within a night. This emission is strongest and more peaked to lower velocities in the first spectra of 14/12/1994 and weakest in the last spectrum (16/12/1994). The He I profiles follow the behaviour of sodium in a similar manner as detected in the October 1993 spectra. The He I absorption wings are weak and extended to the red when absorption longward of Na I *D* starts to appear, and are stronger

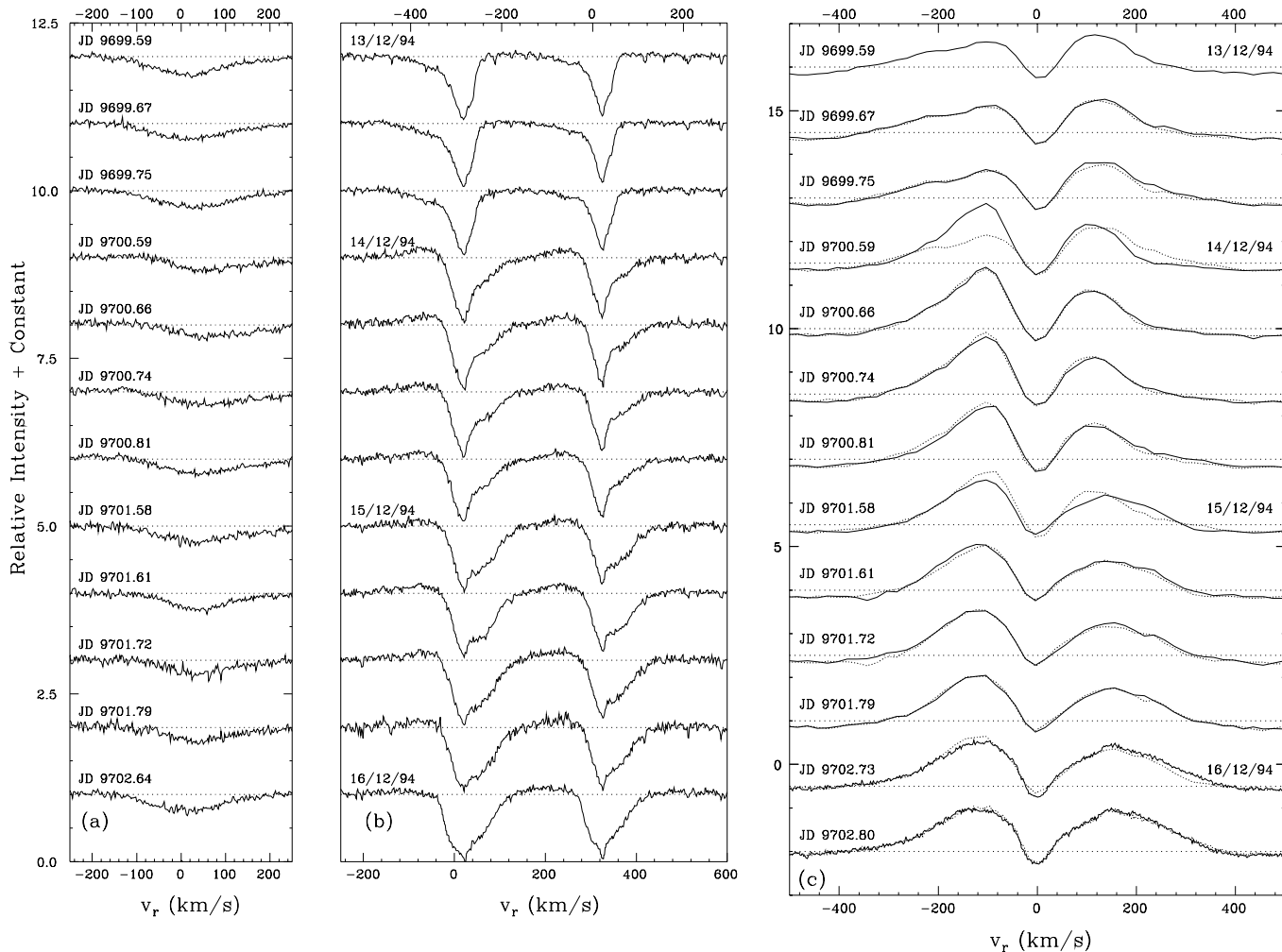


Fig. 4. **a** He I and **b** Na I D high resolution line profiles, and **c** H α high and intermediate resolution line profiles of BF Ori, all taken exactly simultaneously between December 13–16, 1994. The continuum levels are again indicated by thin dotted lines as in Fig. 1c. To visualize the variability the preceding spectrum is plotted by dots.

in absorption but less extended to the red when the RAC structures develop. The appearance of extra blueshifted absorption during 16/12/1994 is also seen in the He I profile. Finally, the H α profiles show an unexpected event; flipping over the strengths of the V and R peaks. During 14/12/1994 the blue peak increased in strength, a comparable profile as observed on 11/01/1994, Fig. 3. The red peak is significantly less extended to the red, but in strength equivalent as before. On 15/12/1994 the red peak became less prominent but well extended to high velocities. The blue peak did not change very much, but diminished a bit. These last two effects also continue during 16/12/1994 weakly.

4.2.2. The intermediate resolution 6260–6860 Å spectra

Several strong absorption lines of Si II and Fe II are identified, see Fig. 5. These lines are narrow (2–3 Å in equivalent width) well known shell lines, although the silicon lines are unusually strong. The detected features are quite stable in strength and profile throughout the observations compared with the Na I,

He I and H α lines. This is the reason we only have shown the averaged spectrum for each night in Fig. 5. Remarkable is the detection of another weak He I line at 6678 Å. Unfortunately this line is weak and the resolution too low to make a proper analysis.

5. The spectral features discussed

5.1. Evidences for extra-solar cometesimals

5.1.1. The sodium resonance lines

Most observed profiles and (dynamical) characteristics of the sodium lines appear identical to those observed for UX Ori (Grinin et al. 1994). We, therefore, propose a similar origin by infalling (solid) bodies that evaporate when approaching the star. Furthermore, neutral sodium does not survive for more than a few seconds near an A-type star (Sorelli et al. 1996). When it is observed for longer periods it is proposed to come from the continuous and complete evaporation of meter-size bodies (Grinin et al. 1996b).

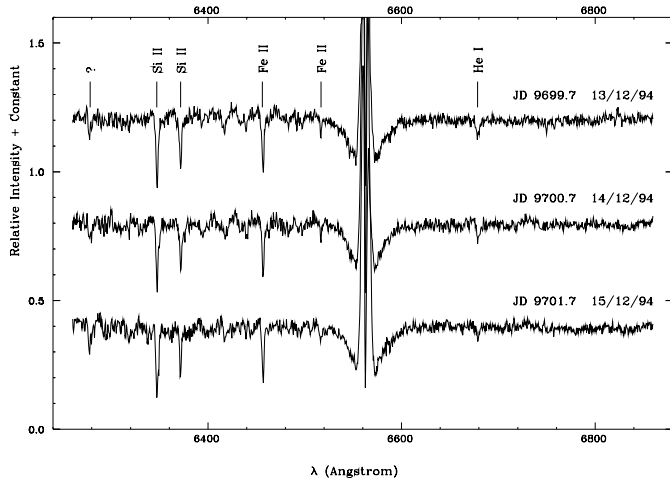


Fig. 5. The 6260–6860 Å intermediate resolution spectra. For each night we show the averaged one of 3 or 4 spectra taken between December 13 and 15, 1994. The following sharp weak and strong absorption lines are identified: Si II (2) 6347.1 and 6371.4 Å, Fe II (74) 6456.4 Å, Fe II (40) 6516.1 Å and He I (46) 6678.1 Å. The line at 6278.3 Å and several weak broad absorption features could not be identified.

Blueshifted sodium components present in BF Ori are not observed for UX Ori. Grinin et al. (1996a) explained the appearance of blueshifted emission, in such a case, as being part of an inverted P Cygni profile, caused by longer time scale accretion than the RACs events. This is inconsistent with: (a) our observed time scales of these changes, being not different as for the RACs; (b) the emission may be also absent when redshifted absorption is observed, and (c) an inverted P Cygni profile does not explain the almost discrete change from blueshifted absorption to emission in one day during the December 1994 sequence.

Model calculations by Grinin et al. (1996b) show that blueshifted emission lines are expected when the evaporation is efficient and the gaseous tail is swept up by the radiation pressure of the central star. If the gaseous tail material is still dense, absorption will appear blueshifted, e.g. in the 10/10/1993 spectrum, or it depresses the shortward emission. Support for this mechanism is the strong RAC (an evaporation event) the night before (09/10/1993). We expect then the reappearance of the blueshifted emission when the density decreases again the day after, as detected in the 10 to 11/10/1993 sequence. In contrast to this, the sodium profile of 12/10/1993 shows a shortward absorption component and emission even more to the blue, not preceded but followed by a RAC. It might be that we undersampled this RAC occurrence. In view of the 08 to 10/10/1993 RAC event this seems hardly plausible. We, therefore, consider other (additional) mechanisms to explain the blueshifted absorption and emission components of sodium.

The calculations of Grinin et al. (1996b) and Sorelli et al. (1996) showed that the radiation pressure is so efficient in accelerating atoms from the evaporated material that the infall motion is turned in an outflow motion within 10^5 s for 1 m sized bodies, giving evaporation densities for n_H of 10^{12} to 10^9 cm $^{-3}$ from solar to comet like abundances. Consequently, it was even ques-

tioned why red shifted absorption lines are observed at all. Our observations show that blueshifted line features are present, but about 1/10 to 1/5 in strength of the RACs. This supports these model calculations but also indicates that the calculated values of the densities must be significantly lower, given that the radiation pressure is a stable value. Either the proposed evaporation or the desintegration processes are less efficient than proposed in these studies. Incomplete evaporation is well known to happen for solar system comets too.

Infalling material in or coming from the back side of the disk will produce also blueshifted features if visible. The evaporation of a star-grazer out of the line of sight can only be detected when emission is produced, as explained for the gaseous tails. Such blueshifted emission will appear weaker than the RACs, as observed. Blueshifted absorption component (BAC) can become visible if an evaporating body crosses the line of sight, after or close to its periastron passage. In such a case, the periastron itself can be located outside the line of sight or even in the line of sight. In fact, the key parameter is the longitude of periastron W defined as 0° when aligned along the line of sight, in the observer-star direction (see Fig. 6). BACs are due to bodies with $W \approx 180^\circ$ and RACs to bodies with $W \approx 0^\circ$. However, observing a BAC requires the corresponding body to survive a more or less long time after periastron passage, and that the passing distance still permits evaporation. The most favourable (and realistic) situation is achieved for $W \sim 180^\circ$, i.e., the periastron located in the line of sight (see Fig. 6). Such a body would be first be visible as a BAC when entering the line of sight, and as a RAC when leaving the line of sight. Again, it might be followed by the blueshifted tail emission. As explained by Kholtygin et al. (1997) the RAC is more dispersed in velocity range than the original BAC. This effect also depends on the periastron distance Q , the eccentricity of the orbit and the velocities of the objects, see Fig. 6. The shorter the periastron passage takes, the larger the velocity shifts and the smaller the delay of a RAC following a BAC. For a periastron passage a correct time scale is of the order 10–20 hours, given the observed October 1993 BAC and RAC characteristics. Another point to note here, is that the sum of the covering factors for both BAC and RAC when caused by one transit object, may not exceed the 100%. If so, the events are due to two different bodies or separate fragments of the same initial body.

We might have detected two of such events, BACs preceding RACs. Note the sodium profiles in the 12 to 14/10/1993 and the 17 to 20/08/1994 sequence. Only in the latter the shortward emission is very weak. However, we expect that BACs are not as frequently observed as RACs or that they produce weaker lines for the following two reasons: (1) as suggested by Grinin et al. (1996b) and Beust et al. (1996) evaporating bodies are disrupted in smaller pieces, e.g. the Shoemaker-Levy impact on Jupiter. We suspect, therefore, a situation similar as in the solar system, that most cometaries are not periodic but are disrupted during one passage and/or collide with the star; (2) the studied systems are very young, the disk is not tenuous and therefore, enhances the disruption of a star-grazer by friction and collisions (causes of the He I lines, see Sect. 5.1.2.). It is, therefore, possible that

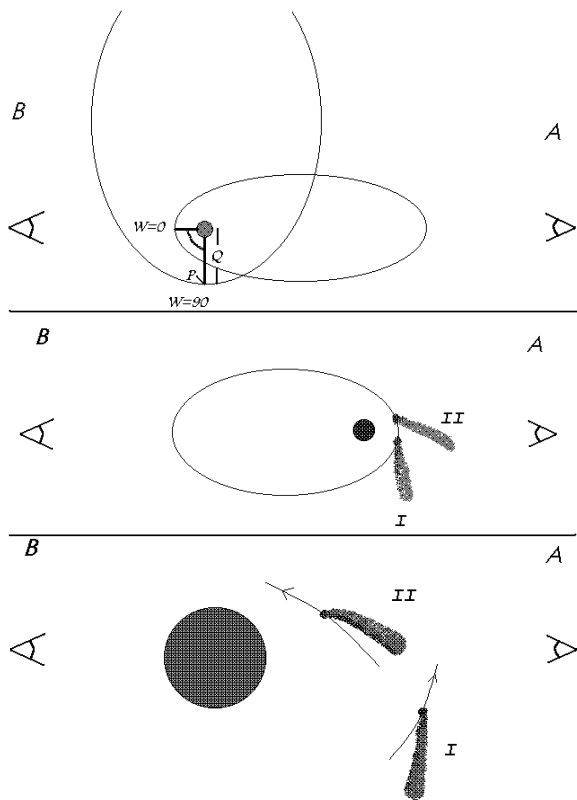


Fig. 6. A hypothetical arbitrary presentation of possible orbits of cometaries as proposed in the text. The cometaries may describe only a part of the orbit as the evaporation might be that efficient that no complete orbit can be fulfilled. Furthermore, the cometary may be disintegrated in many smaller parts, as discussed by Grinin et al. (1996), or collide with the central star, alike the Shoemaker-Levy event. We present here: (*top:*) definition of some orbits and orbital parameters such as the periastron (P), periastron distance to the central star (Q) and the periastron longitude (W) defined as 0° when being the extension of the line of sight seen from position A). We assumed that the inclination of the cometary orbits and the line of sight is around 0° . (*middle:*) The situation in which an RACs is preceded by a BACs, as fully described in Sect. 5.1.1. and when seen from position A). In these situations the tail, being swept up by radiation pressure and stellar wind, may only be presented by blueshifted emission. When being situated in position B) no absorption components but only the tail emission is again seen. (*bottom:*) A more detailed presentation in which cases RACs (II) and BACs (I) sodium components are seen when the observer is in position A). Note that these features may be seen in any part of the orbit, as drawn in the above figures, when the evaporating body is in the line of sight. To observe BACs, however, the cometary must have had survived a closer to stellar part of the orbit than the object causing RACs, a reason, probably, that RACs are more frequently seen. From observers position B) only the tail emission (I & II) might be seen blueshifted, as it is probably been swept up, as noted above.

a RAC following a BAC is due to different star-grazers or fragments. This will certainly be the case when separated a few days in a periastron passage of which the timescale is of the order 10–20 hours, as noted before. In our observations different star-grazers or fragments might have been the origin of the BAC to RAC evolutions from 12 to 14/10/1993 and 17 to 20/08/1994.

Finally, we must consider an origin of the blueshifted components due to the stellar wind as for the UV features (Grady et al. 1996). We expect then these components to appear independent of the infall activities, which is not the case. It may be that the wind features are suppressed during infall activities. This is difficult to understand as various spectra with low accretion activities, see also those in Grinin et al. (1996a), hardly contain blueshifted (wind) absorption. On the contrary, when RACs are present blueshifted emission is observed, possibly arising from the comet tail swept up by the stellar wind.

In the time series of the August 1994 spectra, we detect variable sharp strong absorption, accompanying and blending the interstellar absorption at the blue and red side. These low velocity lines are observed in UX Ori (Grinin et al. 1994) and are most pronounced when the star is at maximum brightness and RACs are present. The velocities of the strongest sharp absorption lines in each data-set, normally identified as the interstellar component, are not similar. This suggests that the real interstellar line at LSR of Orion is blended by the various very sharp deep absorption lines. We interpreted them as caused by cold, slow moving, dense and clumpy gaseous material (partly) in the line of sight, and might be identified as orbiting evaporating bodies. The disruption of such clumps (Grinin et al. 1994) may be the origin of the infalling material. More monitoring data are necessary to support this as more explanations are possible, see Sect. 5.2.

5.1.2. The helium absorption lines

The observed He I absorption lines, Figs. 1a, 3a and 4a, cannot be of photospheric origin as BF Ori is of spectral type A and because of the detected day-by-day variations. These changes of intensity, line profile, and velocity range strongly co-vary with the accretion events. In analogy with UX Ori, we propose that they originate from collisionally ionized gas caused by the interaction of the infalling matter with inner disk material (Grinin et al. 1994; de Winter et al. 1994). The rapid changes of velocities and direction, especially seen in the December 1994 data (Sect. 5.2), exclude that the absorption is due to the stellar wind.

Note that the He I absorption line is also present in variable strength when accretion observed by the sodium lines is almost absent (Fig. 4). Grinin et al. (1996a) explained a similar detection by accretion being different from the star-grazers events, being also the cause of the blueshifted emission in the sodium lines. However, we detected at least some He I absorption in all spectra of BF Ori. A more stable situation is the presence of a hot, kind of boundary, layer produced by the accreting material. This layer might not be restricted to the near circumstellar environment but also around all kind of (accreting) clumpy material that is “ploughing” through the disk.

An additional explanation is that volatiles, such as He I, are released by evaporation when trapped in clathrate structures (Grady et al. 1998). But again such a mechanism explains only the He I variations when accompanied by other, observed, evaporated products, such as Na I.

5.1.3. The $H\alpha$ emission line

Herbig Ae/Be stars have very complex and variable $H\alpha$ profiles (Fernández et al. 1995; Reipurth et al. 1996). Probable mechanisms that may explain those for BF Ori, Figs. 1c, 3 and 4c, will be discussed here.

First, the “standard” strong and broad double peaked $H\alpha$ profile for HAeBes is explained by Kholtygin et al. (1997). Here the main emission is formed in a shell with a stellar wind of which the velocity law can be described by a standard Lamers law. Then emission up to 250 km s^{-1} is formed within $9 R_*$, with $v_\infty = 400 \text{ km s}^{-1}$, as being the maximum value at which emission is still observed in the BF Ori case. However, the $H\alpha$ profile can be dominantly influenced by accretion, note the reversed P Cygni profile of $H\alpha$ for UX Ori (Grinin et al. 1994). Although for both stars similar RACs in the sodium lines are detected, such straightforward evidence of accreting gas is not detected for BF Ori. It seems that no direct relation for both accretion detections exists. This might be evident as the $H\alpha$ emission is formed closer to the star than features due to material from evaporating bodies, see Sect. 6.

Second, obscuration of the $H\alpha$ emission region by large dust clouds during strong photometric minima was first detected for UX Ori and determines the resulting profile (Grinin et al. 1994). The double peaked emission line then appears as a weak single peak, as the direct line of sight to the star is blocked and only emission radiation from the shell or disk is visible. A similar event for BF Ori, during October 1993, Fig. 1c, shows that the star was at intermediate brightness with the self-absorption component being much weaker than observed at brighter stages such as January 1995, Fig. 3c. Also the total emission is less than at maximum brightness, but normalized to the weaker continuum it might occur relatively strong as perfectly observed for UX Ori (Figs. 3 & 4 in Grinin et al. 1994). This normalization effect may explain the high emission volume observed in Fig. 1c compared to those observed at other epochs. Due to this artefact, the same amount of gas in infalling material might result in stronger variations in minima than at brighter stages. On one hand the self-absorption peak follow the large changes in light level which seems both to be stable during monitoring runs and might have been stable from December 1994 until January 1995. On the other hand also rapid large photometric changes are known for BF Ori. In this way obscurations can influence indirect the shorter time scales variations of $H\alpha$ too. Note for instance the different self-absorption components on 8 and 12/10/1993. Moreover, the self-absorption peaks seems to be stable during monitoring runs and might have been stable from December 1994 until January 1995.

Third, the evaporated material from the star-grazers will cause extra $H\alpha$ redshifted absorption components equivalent to the RACs of the sodium lines. Such variations are seen by the co-variation of the red peak with the sodium RACs in all of the $H\alpha$ profiles. In case of the same origin and same covering factors, the strength of these variations compared to those in the RACs of sodium will depend on their relative abundances and transition probabilities. We assume that the transitions originate

from material just released from solid-state, so neutral and with mostly non-excited atoms, in the same physical conditions. The transition probabilities are approximately 3/1/1 for Na I D doublet/ $H\alpha$ /He I 5876 triplet in case the first excitation levels are well populated, if not the ratios are up to 3/0.1/0.1. The relative estimated averages of the amplitude of these variations are 2×1.3 for Na I/H I and 2×2.0 for Na I/He I. Although individual estimates differ and the picture is simplified, it is clear that $[\text{Na I}] > [\text{H I}] > [\text{He I}]$ in relative abundances in our first approximation, or in the second at least equivalent, but in any case not comparable with cosmic abundances. We want to add here that the assumption of similar covering factors for the species considered is an assumption of equal radiation pressures. Although, the radiation pressure still plays a crucial rôle in the evaporation process as noted in Sect. 5.1.1.

Good examples for such redshifted absorption components occurred in the blue $H\alpha$ peaks of the January 1995 spectra, Fig. 3. Unfortunately, no sodium lines are observed for comparison. In this time series the absorption peak first increases in strength and velocity, from -80 (15/01/1995) to -100 km s^{-1} (16/01/1995), and diminishes continuously the following 4 days. When the radial velocity of the absorbing material is close to the self-absorption peak at $+17 \text{ km s}^{-1}$, e.g. 19/01/1995, both the blue and red emission peaks show a similar absorption component, here at about 50 km s^{-1} away from the self-absorption component. Note that the $H\alpha$ emission originates from the direct stellar environment. Star-grazers are, therefore, also visible in $H\alpha$ if they evaporate between this emission region, about $9 R_*$, and the observer. Thus they are also observable more frequently and in different regions of the disk than when observed in the Na I D lines.

Fourth, as most of the $H\alpha$ emission is formed in the vicinity, $< 9 R_*$, of the central object, rotational effects must be taken into account also. The rotational period of BF Ori is about 3 days, derived from $v \sin i \sim 100 \text{ km s}^{-1}$ (Böhm & Catala 1995) and R_* (Sect. 6). Such effects are then difficult to separate from any accretion effect, without the help of other, simultaneously observed, lines. For example the co-variations with the sodium RACs, but also the relative weak changes in the blue $H\alpha$ emission peaks for BF Ori and UX Ori on this time scale (Grinin et al. 1994; de Winter et al. 1994), are reasons to exclude a pure rotational origin. Rotation though could explain the behaviour of the January 1995 absorption components in the emission peaks when dense material close to the star is dragged into similar rotations.

Rotation of the $H\alpha$ emission region might even strengthen the current complexity. For example, in case the evaporating bodies will move in a similar direction as the star and the co-rotating $H\alpha$ emission region, they will obscure the redshifted part of the $H\alpha$ profile at lower velocities than the blue peak. As the emission peak lies at low velocities, this means relatively stronger absorption in the red than in the blue. Such an effect may be visible during the 08 to 09/10/1993 obscuration, in the latter the emission ranges up to $+250$ and to -300 km s^{-1} , when the RACs, i.e. the screening, is the strongest. When getting brighter the emission extends to higher velocities, up to $+350$

and -350 km s^{-1} in the spectra of 10 and 11/10/1993. This is followed the 12th by a stronger decrease at higher velocities of the blueshifted emission peak than in the red. The later being in accordance with the blueshifted absorption of *sodium* that night. We suggest, therefore, “co-rotation” of the accretion process with the star or local environment. Moreover, that during the infall of much material part of the $\text{H}\alpha$ velocity field is screened, which is then “biased” to lower velocities.

Fifth, in the case that evaporated gas from infalling bodies causes $\text{H}\alpha$ variations, blueshifted events as observed for sodium must be seen also. This would explain the differences in the self-absorption profile between 11 and 12/10/1993. A reason to observe blueshifted emission, as discussed for the sodium lines, is the result of evaporated material swept up by the stellar wind and radiation pressure. Indeed, the dramatic weakening of the blue peak at 10/10/1993 follows the strongest RACs of the days before. Hydrogen gas produced by evaporation will survive the stellar radiation field longer than neutral sodium. Therefore, $\text{H}\alpha$ features are in general stronger, easier to detect and useful to explain the blueshifted sodium events.

For example, in the case where we mentioned the occurrence of extra emission, around -200 km s^{-1} , in the 11/10/1993 spectrum. It is preceded by emission at higher velocities and disappears the day after. Again this emission feature follows the strong RAC of sodium, so a connection with a star-grazer is tempting. The velocity is close to the maximum velocity for the accreting sodium. When the star-grazer is out of the line-of-sight its gaseous material could be seen as emission, hydrogen will “survive” longer. So, such an observable accretion effect does not have to show similar features in Na I and $\text{H}\alpha$.

Without simultaneous guiding Na I D spectra $\text{H}\alpha$ profiles are hard to understand, e.g. the 11/01/1994 spectrum (Fig. 3). In this spectrum the $\text{H}\alpha$ emission peaks are flipped in strength compared those shown in Figs. 1c and 3. Similar profiles were detected during December 1994, see Fig. 4, and will be explained in the following section.

5.2. Spectroscopic evidences for revolving clouds

Photometric minima of UXOR type stars are explained by the obscurations by large optically thick dust clouds. Supporting spectroscopic evidences for UX Ori (Grinin et al. 1994) seem also to be present for BF Ori during the intermediate brightness phase in October 1993. The spectroscopic absence of any strong additional component in the observed lines shows us that the obscuring material is not very gaseous. In the case that the dust to gas ratio is very low, we then expect evidences for revolving clouds, which will be addressed now.

A clear difference between BF Ori and UX Ori is the V/R ratio of most $\text{H}\alpha$ profiles, mainly < 1 for BF Ori and > 1 for UX Ori. For $V \neq R$ and variations therein, could be explained by the presence of a density structure in the disk. When it rotates a flip over of the peaks is observed (Telting et al. 1994). A flip over of the V/R value for the $\text{H}\alpha$ profiles was detected both during December 1994 and January 1995, it happened only once per time series and lasted at least two days. The time scale must

be at least of the order of weeks and excludes an explanation exclusively based on stellar rotation.

Simultaneous with the flip over in $\text{H}\alpha$, during the December 1994 observations, absorption components of Na I D and He I changed from blue to redshifted, Fig. 4. This proves again a common origin of the line forming regions. We use the absorption/obscuration hypothesis of the previous sections to explain this behaviour. The $\text{H}\alpha$ emission is formed much closer to the stellar surface than the distance where the star-grazers evaporate. The continuous evaporation of refractories in the gaseous tail, cool gaseous material, causes the Na I D absorption and the hot collisionally ionized gas the lines of He I . On 13/12/1995 the cool material moves towards the observer but the hot He I region is roughly at systemic velocity with a more extended wing in the red. The day after, the Na I D and He I features are followed by similar profiles but clearly redshifted. The blueshifted absorption in sodium changed to weak emission. In case of He I the blue part may be filled in by some emission too. This emission might have been present before and was explained earlier by swept up gas from the evaporation process. The almost instant change of velocity in both the cool and hot regions indicates that the absorbing material causing this is rather clumpy.

The evaporated gas of this clump or body absorbs part of the $\text{H}\alpha$ emission. It does not explain why this absorption is peaked to higher velocities than for sodium though. It might be that the absorbing hydrogen covers a larger region than the sodium, as mentioned in Sect. 5.1.3. If due to a higher hydrogen abundance the ratio must be 0.6 for $[\text{Na}/\text{H}]$ and for $[\text{Na}/\text{He}]$ roughly 2, but note the simplified picture of these estimations as discussed in Sect. 5.1.3. point three, and that parts of the absorption might be filled in with emission.

When the absorbing body changes its direction of movement from towards us to away from us, it will not absorb in the blue anymore. Reasons for the increase of the violet $\text{H}\alpha$ peak. The change seen in the red $\text{H}\alpha$ peak is less extended emission, being cut-off at 220 km s^{-1} instead of at 260 km s^{-1} . The latter again strongly supports our obscuration and co-rotation hypothesis: the absorbing body is now seen more in the line-of-sight, covering only the $\text{H}\alpha$ emission regions closest to the star that co-rotates, only the red wing diminishes at higher velocities. In another way, it is hard to explain influences on the $\text{H}\alpha$ profile in the blue and red over a velocity range of about 500 km s^{-1} in one day. From the center of the He I profiles and wings of the sodium lines we estimate that this body or clump itself changed about 70 km s^{-1} in radial velocity in one day.

The third night (15/12/1994) the sodium lines are stronger and peak to lower velocities, the latter is also seen for the He I line. Probably more cool gaseous material is produced in the line of sight. This extra material causes also extra absorption in $\text{H}\alpha$ at low velocities. As the body moves around the central object, and is now seen further out the line-of-sight, parts of the $\text{H}\alpha$ emitting region close to the star will be less obscured, the red wing at higher velocities is indeed stronger again.

The observed properties and changes in this data-set are very different from those observed before. In view of these data we propose a larger body that moves in a wider orbit but of which

material is evaporating and falls to the star as the red absorption wings get more pronounced. This body must be partly gaseous, for the absorption components, and partly dusty, for the obscuration.

6. Size of the October, 1993, comet-like body

With the different data-sets we have solved the time scale of the accretion events. Consequently, we can interpret the increase of strength of the RAC, on 8 and 9 October 1993, and the disappearance during the following nights as accretion of cool material in a certain concentration or clumpy structure. As we proposed this to be a comet-like evaporating body we can estimate: (1) its size and mass when it is or becomes (by evaporation) completely gaseous, and (2) the distance to BF Ori when evaporation takes place.

The optical depth can be written as

$$\tau_\nu = \frac{\pi e^2}{m_e c} N f Q_{abs}(\nu) \quad (1)$$

in which e and m_e denote the charge and mass of an electron, respectively; c is the light speed; N is the number of absorbing atoms per cm^3 in the energy level from which the absorption occurs; f is the oscillator strength and Q_{abs} the absorption efficiency.

The absorption efficiency

$$\int_0^\infty Q_{abs}(\nu) d\nu \approx 1 \quad (2)$$

for absorption at most dust materials around A-type stars with grain sizes $a \gg 10^{-5}$ cm (Gilman 1974). As BF Ori was observed at a relatively bright phase, either the optical depth of the absorbing material was not too large, option (1), or the stellar surface was only partly obscured, option (2). Option (2) seems more realistic as the relative strength of both sodium lines are equal which points to saturated lines, so optically thick gas. As the RACs go down to roughly 0.5 of the continuum level we estimate a 50% projected covering of the stellar surface by the evaporated gas. We shall, however, start our calculations with option (1) being the first approximation.

Option (1): For the Na I D RACs of 9 October, 1993, we can estimate $\tau_\nu \approx 0.5$ compared to the component at rest velocity. The amount of evaporated sodium particles from this infalling body can then be estimated from

$$\int \tau_\nu d\nu \approx 0.5 \Delta\nu = \frac{\pi e^2}{m_e c} N f \quad (3)$$

The material detected in the RACs is shifted by about 100 km s^{-1} , so for the D_2 line at 5890 \AA the $\Delta\nu = v/\lambda$ can be calculated. As the transitions from the ground state of Na I to the first upper term are single and strong we can put for the Na I resonance lines approximately $f = f_{D_2} + f_{D_1} \approx \frac{1}{3} + \frac{2}{3} = 1$. We then obtain for the D_2 line

$$N_{NaI} \approx 9.7 \times 10^{12} \text{ atoms cm}^{-2} \quad (4)$$

in the line of sight on October 9, 1993. For the abundance of sodium we adopt two values: (a) the normal IS abundance

Table 2. Estimated parameters, see text, for a clump of material that causes by complete evaporation the 9 October 1993 RACs. The calculations are done for the IS and comet Halley's abundance. The errors in r_c proceed from the ones in the stellar radius.

Abund.	N_H	$N_H^{Tot.}$	M_c^H	$M_c^{Corr.}$	r_c
Na/H	cm^{-2}	atoms	g	g	km
2×10^{-6}	4.5×10^{18}	2.8×10^{42}	4.5×10^{18}	—	10 ± 2
5×10^{-3}	1.8×10^{15}	1.2×10^{39}	1.8×10^{15}	3.6×10^{16}	2.0 ± 0.4

(Na/H $\approx 2 \times 10^{-6}$), which gives an upper limit for the amount of hydrogen; (b) the dust abundance for material evaporated from comet Halley (Na/H $\approx 5 \times 10^{-3}$), as we have indicated the non cosmic abundances for the evaporated material. (Our abundance estimates itself are not useful, they are very rough values and the absolute influences of the evaporated material on especially $H\alpha$ can not be properly made, note the line complexity and the many influences as discussed.) For each abundance we have listed in Table 2: (1) the estimated amount of hydrogen ($N_H \text{ cm}^{-2}$) released by the evaporation, (2) with $\log L_*/L_\odot = 1.37_{-0.13}^{+0.11}$, $\log T_{eff} = 3.90$ (Sect. 2) we get $R_* = 6.2_{-1.6}^{+1.8} R_\odot$, and obtain $N_H^{Tot.}$, being the total amount of hydrogen atoms in the line of sight when the evaporating material obscures the whole stellar surface, (3) the hydrogen mass of the evaporated material: M_c^H and (4) $M_c^{Corr.}$, the mass M_c^H corrected for the overabundance of heavy elements for comet Halley's abundances (Jessberger et al. 1988).

The masses derived are comparable to those of comets in the solar system. The radii of the evaporating cloud (r_c), given in Table 2, are estimated from:

$$r_c^3 = \frac{3M_c}{4\pi\rho_c} \quad (5)$$

and the cometary density $\rho_c \approx 1 \text{ g cm}^{-3}$, similar to the density of the outer planets in the solar system.

When the evaporating material obscures only 50% of the stellar surface the size will be about 8 to 1.6 km, instead of the values given in Table 2.

Option (2): This option is now easy to describe as the latter numbers will change to >8 and >2 km, for respectively the cosmic and mass corrected Halley's abundances, in the 50% covering approximation *but* with an optical depth of $\tau_\nu \gg 1.0$ taken.

Because $r_c \sim \rho_c^{-1/3}$, different densities only play a crucial role when our solid body approximation is wrong. For higher optical depths, M_c will be an equivalent factor higher. As a general result we have in the solid approximation evaporating bodies which are at least solar-type comets in their sizes and masses. Assuming that such "cometary" are falling straight toward the star, along the line of sight, the evaporation will take place at a distance

$$r_d = \frac{2GM_*}{v_{esc}^2} \quad (6)$$

with $v_{esc} \approx 100 \text{ km s}^{-1}$ and $M_* = 2 M_\odot$ we get

$$r_d \approx 0.4 \text{ AU} \quad (7)$$

This value can be used as a rough indication of typical values to consider. In a more realistic case the cometary crosses the line of sight with some projected observed velocities, being in this case $\approx 100 \text{ km s}^{-1}$. The deduced 0.4 AU is, therefore, only an upper limit. In case the RAC is caused by fragmentation, as discussed for our October spectra, from an orbiting body as detected in the December 1994 monitoring programme, this “parental-body” must have been orbiting at a larger distance than estimated, so at least 0.4 AU ($\approx 14 R_*$). The period of a comet orbit would then be at least 65 days for zero eccentricity.

We have detected another revolving body, in Sect. 5.2., to move from one side of BF Ori to the other, or $12.4_{-3.2}^{+3.6} R_\odot$, within 1.8 days. Adopting a Keplerian orbit we obtain a period of 80 ± 20 days for such a body if periodical, with distance $a = 0.46 \pm 0.11$ AU. Possible follow-up observations must therefore include a monitoring programme covering these time scales.

7. Comparison with other Herbig Ae/Be stars

Routine detection of infalling, circumstellar gas in all of the UXORs with high resolution optical or UV data suggests that infall episodes are frequent in the disks of Herbig Ae stars. Recent UV studies of AB Aur ($\log(\text{Age}/\text{yr}) = 6.3 \pm 0.2$, van den Ancker et al. 1997, 1998) and HD 163296 ($\log(\text{Age}/\text{yr}) = 6.6 \pm 0.4$) suggest that infalling circumstellar material is visible at all epochs in AB Aur (Grady et al. 1998) while more sporadic, about 25% for the time sampled, for the slightly older HD 163296 system (Grady et al. 1999). The still older HD 100546 system (age > 10 Myr), despite very limited UV temporal coverage, shows distinct strong/weak infall episodes (Grady et al. 1997), similar to those observed in β Pic. The level of infall activity for BF Ori, about 60% of the observed nights, with pronounced night-to-night variations as well as some indication of short duration quiescent periods, appears intermediate in character between AB Aur and HD 163296.

8. Model interpretations and results

The study of spectroscopic features which can be interpreted arising from (solid) star grazing bodies, as observed in UX Ori, motivated the spectroscopic monitoring of BF Ori at different epochs and wavelength regions including the He I 5876 Å, Na I D and H α lines. The selection of BF Ori is based on its similarities with UX Ori. Both are Herbig Ae stars of the same age, 3_{-1}^{+2} Myr, belong to the UXOR subclass, and are known to have many observational phenomena in common. The following similarities between BF Ori and UX Ori are observed in our time series:

-) Very extended red wings in the Na I D lines. Sometimes seen as complete redshifted absorption components (RACs).
-) The existence of He I λ 5876 in absorption, and co-variations with the redshifted absorption Na I D profiles.
-) A double peaked H α emission profile. Although for BF Ori the red peak is the strongest in most spectra, while for UX Ori

V/R > 1 , the day-to-day variations of this profile are similar and in phase with those seen for the Na I D lines.

Most observed spectroscopic properties in BF Ori can be explained by the detection and dynamics of two types of CS bodies, namely by the presence of extra-solar comets and revolving dust clouds. Both mechanisms are separately discussed below.

8.1. Detection of extra-solar comets around BF Ori

In agreement with observations of UX Ori (Grinin et al. 1994; de Winter et al. 1994), some other UXORs (Grinin et al. 1996a; Grady et al. 1996) and theoretical studies (Sorelli et al. 1996; Beust et al. 1996; Grinin et al. 1996b; Khoitygin et al. 1997) our monitoring data strongly supports the general interpretation that we observe the evaporation process of solid star-grazers, based on the following arguments:

- 1) Neutral atomic gas species near an A-type star have a short photoionization lifetime (Sorelli et al. 1996). This indicates the *in-situ* production of Na I at free-fall velocities as detected.
- 2) These high velocity redshifts of several hundreds of km s^{-1} rule out a more classical grain transport process such as the Poynting-Robertson drag and an origin in small grains. Radiation pressure will rapidly remove grains below a few microns from the stellar vicinity (Sitko et al. 1994).
- 3) The infalling material is clumpy and not ionized. We resolved in our time series that infall events last several days with strong variations, and the absence of infall in some occasions. This disagrees with a more continuous accretion and mechanisms considered, such as magnetospherically channeled accretion (Edwards et al. 1994).
- 4) The presence and the variations of He I absorption cannot be accounted for by the photosphere of an A-type giant. It is explained, note the co-variations, by collisionally ionized gas produced by interaction of the infalling material with the disk material. Other explanation are discussed, such as He I released from icy clathrates (Grady et al. 1998), but these do not fully explain the observations.
- 5) The H α profile changes are very complex, but can be explained as absorption by the evaporated material, e.g. the gaseous comae, and obscurations of the H α emission line forming region, extending up to 0.2 AU, by the infalling bodies and clumpy (partly evaporated) material at larger distances.
- 6) The equal structure and strength of both the RACs of the sodium D components indicate the presence of optically thick gas. Together with the flat-bottomed absorption and the covering factors it supports that significant parts of the stellar surface, up to about 50%, are obscured.
- 7) The resolved time scale of the infall events suggests that we witnessed the evaporation of one infalling clump from 8 to 10 October 1993. Calculations show that this “cometary” had a possible mass of 3.6×10^{16} – 4.5×10^{18} g and a size of 2–10 km when completely evaporated and depending on the abundances taken. The distance to the central star during evaporation was in the order of 0.4 AU.

8) The determined abundances for the infall events are typically not cosmic, $[\text{Na}] \geq [\text{He}] \geq [\text{H}]$. The presence of refractory elements and their high ratio against the volatiles, as best observed in the UV (Grady et al. 1996a), constitutes evidence for reprocessed material with an origin in grains or larger solid bodies.

This is in fact what we observed: the reprocessing mechanism, the evaporated material, originating from the outer regions, enrich the inner disk material with fresh dust and heavy elements (Grinin et al. 1996b), both required for the formation of true planetesimals. In view of the similar evaporation process with the (reprocessing) comets in our solar system, and the common dimensions as mass and size we prefer to speak about extra-solar comets, cometaries or cometesimals. Additional arguments for this interpretation are given by de Winter et al. (1997).

9) A difference with UX Ori is that we detected for BF Ori blueshifted absorption and weak emission components in the $\text{Na I } D$ lines. We have shown that the blueshifted events are either due to swept up gaseous material, as shown theoretically to occur when the evaporation of the star-grazers is efficient (Grinin et al. 1996b), or due to accretion activities coming from the “back-side” of the disk. With the current data no good distinction between the two can be made.

Referring to cometaries for our detected star-grazers one may expect periodicity and therefore these blueshifted features. We have shown that blueshifted events similar to the redshifted ones are visible, but weaker. Note that for young objects the life time of accreting bodies are shortened as they move through disk-material, as seen by the strong shell lines (Fig. 2). A situation, in general, not very different from that in the solar-system where most comets do not survive a solar passage.

Indeed infall or passage fragmentation will occur as indicated by theoretical calculations (Grinin et al. 1996b; Beust et al. 1996) and visible by the Shoemaker-Levy event. Calculations of Beust et al. (1996) show to a sharp limit in the red wing of the absorption profile when one observes the evaporation of one single body. Indeed the 09/10/1993 spectra show a sodium RACs with a sharp limit at $\sim 120 \text{ km s}^{-1}$, which support the calculations made before. A number of them in the line of sight, with gaseous overlapping velocities, produces a RAC that decreases slowly to higher velocities, e.g. the spectra of 08 and 13/10/1993. We have evidences of both situations. In case fragmentation occurred in the 09/10/1993 case, the parental body was larger than the calculations made for this cometary or fragment. Evidences for large bodies are also found in our spectroscopic monitoring. However, we have discussed in Sect. 5.1.1. that a complete evaporation of 1 m sized bodies desintegrated from a large cometary, as proposed by Grinin et al. (1996b), does not follow our observations. In a way their calculation show a too efficient desintegration process, which might point to a more solid body that “resists” longer.

8.2. Detection of revolving dust clouds

1) The infall activity identified as evaporating star-grazers is observed to be dependent of the light level. It is supporting

evidences that this accretion activity and the obscuring dust clouds are mainly located in different regions of the CS disk.

2) The low velocity components of $\text{Na I } D$ are very strong in absorption, for both UX Ori and BF Ori, but being variable and not always present for BF Ori. They were explained by slow moving dense cool gaseous bodies of which their covering factors and densities determines the line strength as in the case of the “cometesimals”.

3) The strongest support for rotating clumpy gaseous material, though, are found in the most intensive monitoring programme; that of December 1994. Apart from this, we observed the presence of blueshifted absorption in the $\text{Na I } D$ lines that appeared redshifted the night after and developed to more prominent components, similar to the RACs, on the third night. These changes are detected with exact co-variations of the He I absorption profile and a flip over of the red and violet peak strength of the $\text{H}\alpha$ profile, clearly indicating that the variations of these three different lines must have had a common origin of one single body.

The exact changes with the $\text{H}\alpha$ profile can be well explained again by the hypothesis that parts of the inner disk, where the $\text{H}\alpha$ emission mainly originates, are obscured by cool gaseous bodies orbiting BF Ori. The orbital period of this probably large, partly gaseous, body is calculated to be between 60 and 100 days and a distance of $0.46 \pm 0.11 \text{ AU}$. Note here that the self-absorption peak remains stable for $\Delta t \geq 6$ days during several runs and co-variates with the large brightness changes.

These observations support previous detections of clumpy material by photometric and polarimetric monitoring (e.g. Rostopchina et al. 1997). Calculations show that such clouds, with mass $\approx 10^{21} \text{ g}$ and radius $\approx 8 R_{\star}$ resist tidal forces only down to 10 AU (Grinin et al. 1994).

9. Concluding remarks

Assuming that UXORs are PMS stars, an assumption recently questioned by Kovalchuk & Pugach (1997), they are Herbig Ae stars that are slightly more massive than the progenitors of β Pic like systems. It is tempting, but not fully justified yet (Natta et al. 1997), to assume, as shown by the accretion properties, an evolutionary sequence among these objects. Moreover, the recent detection of a centrally cleared region in the CS disk of the 10 Myr A0 V star HR 4796 (Sandage et al. 1998) might have been triggered by planet formation processes. Note that UXORs like BF Ori and UX Ori may end their PMS phases on the MS as \sim A0 V type objects and can, therefore, be considered possible progenitors of the HR 4796 system.

Based upon all the information that we have gathered in this study, plus the inference of types of observed CS bodies, their characteristics and the fact that we have enriched material in these few Myr old systems, we argue that we are looking at accreting and orbiting planetesimals. A future goal must be to carry out further spectroscopic monitoring of additional UXORs or other young objects in order to justify these conclusions. By covering different time scales and epochs, one might gain more

insight in the relations of the (accreting) CS bodies, if present, with planetesimals and the evolutionary status of the systems.

Acknowledgements. We are grateful to Dr. H.J.G.L.M. Lamers for his help in part of the calculations, to Dr. P.S. Thé for carefully reading parts of the text and to Dr. A.N. Rostopchina for providing photometric support during our October 1993 monitoring. We especially thank the referee Dr. H. Beust for his many useful remarks and interesting discussions. D. de Winter & C. Eiroa were supported by Spanish grant PB 94-0165. M.E. van den Ancker acknowledges financial support from NWO/NFRA grant 781-76-015.

References

- van den Ancker M.E., Thé P.S., Tjin A Djie H.R.E., et al., 1997, *A&A* 324, L33
- van den Ancker M.E., de Winter D., Tjin A Djie H.R.E., 1998, *A&A* 330, 145
- Backman D.E., Paresce F., 1993, In: Levy E.H., Lunine J. (eds.) *Protostars and Planets III*. University of Arizona Press, Tucson, 1253
- Beckwith S.V.W., Sargent A.I., 1996, *Nat* 383, 139
- Beust H., Lagrange A.-M., Plazy F., Mouillet D., 1996, *A&A* 310, 181
- Beust H., Lissauer J.J., 1994, *A&A* 282, 804
- Bibo E.A., Thé P.S., 1991, *A&AS* 89, 319
- Boggess A., Bruhweiler F.C., Grady C.A., et al., 1991, *ApJ* 377, L49
- Böhm T., Catala C., 1995, *A&A* 301, 155
- Crifo F., Vidal-Madjar A., Lallement R., Ferlet R., Gerbaldi M., 1997, *A&A* 320, L29
- Edwards S., Hartigan P., Ghandour L., Andrusic C., 1994, *AJ* 108, 1056
- Ferlet R., Lagrange-Henri A.M., Beust H., et al., 1993, *A&A* 267, 137
- Fernández M., Ortiz E., Eiroa C., Miranda L.F., 1995, *A&AS* 114, 439
- Finkenzeller U., Mundt R., 1984, *A&A* 55, 109
- Gilman R.C., 1974, *ApJS* 28, 397
- Grady C.A., Pérez M.R., Bjorkman K.S., Massa D., 1998, *ApJ*, submitted
- Grady C.A., Pérez M.R., Bjorkman K.S., Massa D., 1999, *ApJ*, to be submitted
- Grady C.A., Pérez M.R., Talavera A., et al., 1996, *A&AS* 120, 157
- Grady C.A., Sitko M.L., Bjorkman K.S., et al., 1997, *ApJ* 483, 449
- Graham J.A., 1992, *PASP* 104, 479
- Grinin V.P., Kiselev N.N., Minikhulov N.H., Chernova G.P., Voshchinnikov N.V., 1991, *Ap&SS* 186, 283
- Grinin V.P., Kozlova O.V., Thé P.S., Rostopchina A.N., 1996a, *A&A* 309, 474
- Grinin V.P., Natta A., Tambovtseva L., 1996b, *A&A* 313, 857
- Grinin V.P., Rostopchina A.N., 1996, *Astr. Rep.* 40, 171
- Grinin V.P., Thé P.S., de Winter D., et al., 1994, *A&A* 292, 165
- Herbst W., Herbst D.K., Grossman E.J., 1994, *AJ* 108, 1906
- Holland W.S., Greaves J.S., Zuckerman B., et al., 1998, *Nat* 392, 788
- Hubeny I., Heap S.R., 1996, *ApJ* 470, 1144
- Jayawardhana R., Fisher S., Hartmann L., et al., 1998, *ApJ* 503, L79
- Jessberger E.K., Kissel J., Rahe J., 1988, In: Atria S.K., Pollack J.B., Mathews (eds.) *Proc. Int. Conf.: Origin and Evolution of Planetary and Satellite Atmospheres*. The University of Arizona Press, Tucson, Az. 167
- Jura M., Zuckerman B., Becklin E.E., Smith R.C., 1993, *ApJ* 418, L37
- Kholtygin A.F., Il'in V.B., Voshchinnikov N.V., 1997, *A&A* 323, 189
- Koerner D.W., Ressler M.E., Werner M.W., Backman D.E., 1998, *ApJ* 503, L83
- Kondo Y., Bruhweiler F.C., 1985, *ApJ* 291, L1
- Kovalchuk G.U., Pugach A.F., 1997, *A&A* 325, 1077
- Kurucz R.L. 1991, In: Davis Philip A.G., Upgren A.R., Janes K.A. (eds.) *Stellar atmospheres—Beyond classical models*. L. Davis press, Schenectady, New York, p. 441
- Lagrange-Henri A.M., Vidal-Madjar A., Ferlet R., 1988, *A&A* 190, 275
- Lanz T., Heap S.R., Hubeny I., 1995, *ApJ* 447, L41
- Mannings V.G., Koerner D.W., Sargent A.I., 1997, *Nat* 388, 555
- Marcy G.W., Butler R.P., 1996, *ApJ* 464, L153
- Mayor M., Queloz D., 1995, *Nat* 378, 355
- Natta A., Grinin V.P., Mannings V., Ungerechts H., 1997, *ApJ* 491, 885
- Palla F., Stahler S.W., 1993, *ApJ* 418, 414
- Reipurth B., Pedrosa A., Lago M.T.V.T., 1996, *A&AS* 120, 229
- Rostopchina A.N., Grinin V.P., Okazaki A., et al., 1997, *A&A* 327, 145
- Shevchenko V.S., Grankin K.N., Ibragimov M.A., Melnikov S.Yu., Yakubov D., 1993, *Ap&SS* 202, 137
- Sitko M.L., Halbedel E.M., Lawrence G.F., Smith J.A., Yanow K., 1994, *ApJ* 432, 753
- Sorelli C., Grinin V.P., Natta A., 1996, *A&A* 309, 155
- Stauffer J.R., Hartmann L.W., Barrado y Navascues D., 1995, *ApJ* 454, 910
- Telting J.H., Heemskerk M.H.M., Henrichs H.F., Savonije G.J., 1994, *A&A* 288, 558
- Timoshenko L.V., 1985, *Astrofizika* 22, 51
- Warren W.H., Hesser J.E., 1978, *ApJS* 36, 497
- Welty A.D., Barden S.C., Huenemoerder D.P., Ramsey L.W., 1992, *AJ* 103, 1673
- de Winter D., Grady C.A., Eiroa C., 1997, In: Rebolo R., Martin E.L., Zapatero Osorio M.R. (eds.) *Proc. Int. Conf.: Brown dwarfs and extra solar planets*. ASP Conf. Ser. 133, 232
- de Winter D., Grinin V.P., Grady C.A., et al., 1994, In: Ferlet R., Vidal-Madjar A. (eds.) *Proc. 10th IAP Meeting: Circumstellar dust disks and planet formation*. Editions Frontières, 171